Acta Biomaterialia 12 (2015) 70–80

Contents lists available at ScienceDirect

Acta Biomaterialia

journal homepage: www.elsevier.com/locate/actabiomat

Functional fabrication of recombinant human collagen–phosphorylcholine hydrogels for regenerative medicine applications

M. Mirazul Islam [a,d,1], Vytautas Cėpla [b,1], Chaoliang He [c,1,2], Joel Edin [d], Tomas Rakickas [b], Karin Kobuch [e], Živilė Ruželė [b], W. Bruce Jackson [c], Mehrdad Rafat [c,d,f], Chris P. Lohmann [e], Ramūnas Valiokas [b,**,1], May Griffith [a,c,d,*,1]

[a] Swedish Medical Nanoscience Center, Dept. of Neurosciences, Karolinska Institutet, S-17177 Stockholm, Sweden
[b] Dept. of Nanoengineering, Center for Physical Sciences and Technology, Savanorių 231, LT-02300 Vilnius, Lithuania
[c] Ottawa Hospital Research Institute – Vision, 501 Smyth Road, Ottawa, Ontario K1H 8L6, Canada
[d] Integrative Regenerative Medicine Centre, Dept. of Clinical and Experimental Medicine, Cell Biology Bldg. – Level 10, Linköping University, S-58185 Linköping, Sweden
[e] Clinic of Ophthalmology, Klinikum rechts der Isar, Technische Universität München, Germany
[f] Dept. of Biomedical Engineering, Linköping University, S-58185 Linköping, Sweden

ARTICLE INFO

Article history:
Received 2 May 2014
Received in revised form 8 October 2014
Accepted 24 October 2014
Available online 31 October 2014

Keywords:
Hydrogel
Cornea
Collagen
Laser profiling
Surface modification

ABSTRACT

The implant–host interface is a critical element in guiding tissue or organ regeneration. We previously developed hydrogels comprising interpenetrating networks of recombinant human collagen type III and 2-methacryloyloxyethyl phosphorylcholine (RHCIII–MPC) as substitutes for the corneal extracellular matrix that promote endogenous regeneration of corneal tissue. To render them functional for clinical application, we have now optimized their composition and thereby enhanced their mechanical properties. We have demonstrated that such optimized RHCIII–MPC hydrogels are suitable for precision femtosecond laser cutting to produce complementing implants and host surgical beds for subsequent tissue welding. This avoids the tissue damage and inflammation associated with manual surgical techniques, thereby leading to more efficient healing. Although we previously demonstrated in clinical testing that RHCIII-based implants stimulated cornea regeneration in patients, the rate of epithelial cell coverage of the implants needs improvement, e.g. modification of the implant surface. We now show that our 500 μm thick RHCIII–MPC constructs comprising over 85% water are suitable for microcontact printing with fibronectin. The resulting fibronectin micropatterns promote cell adhesion, unlike the bare RHCIII–MPC hydrogel. Interestingly, a pattern of 30 μm wide fibronectin stripes enhanced cell attachment and showed the highest mitotic rates, an effect that potentially can be utilized for faster integration of the implant. We have therefore shown that laboratory-produced mimics of naturally occurring collagen and phospholipids can be fabricated into robust hydrogels that can be laser profiled and patterned to enhance their potential function as artificial substitutes of donor human corneas.

1. Introduction

Biointeractive scaffolds designed to mimic the extracellular matrix (ECM) of the body are becoming the scaffolds of choice in regenerative medicine. The interface between implant and host is now recognized as a critical element in guiding the repair and regeneration of target tissues or organs. Biologically inert materials developed as implants for the cornea and other tissue systems can be rendered biointeractive by a range of microfabication techniques. Micromoulding, microfluidics, lithographic patterning and similar processes have already employed for introduction of grooves, channels or other topographical/cell adhesion-promoting features [1–5], or for grafting of interactive peptides [6], growth factors and other bioactives to promote cell attachment and growth [2,7–9]. Biomaterials comprising naturally derived and mimics of ECM components and hybrids of natural and synthetic polymers have also been developed as implants that serve as regeneration scaffold and templates by providing instructive cues

* Corresponding author at: Integrative Regenerative Medicine Centre, Dept. of Clinical and Experimental Medicine, Cell Biology Bldg. – Level 10, Linköping University, S-58185 Linköping, Sweden. Tel.: +46 13 28 1756.
** Co-corresponding author. Tel.: +370 5 2641818.
E-mail addresses: valiokas@ftmc.lt (R. Valiokas), May.Griffith@liu.se (M. Griffith).
[1] These authors contributed equally.
[2] Present address: Key Laboratory of Polymer Eco-materials, Changchun Institute of Applied Chemistry, Chinese Academy of Sciences, 5625 Renmin Street, Changchun 130022, China.

http://dx.doi.org/10.1016/j.actbio.2014.10.035
1742-7061/

to endogenous cells to affect regeneration. A range of biomimetic materials fabricated as hydrogels, membranes, meshes and other structures have now been developed as tissue models and as scaffolds or templates for regenerative medicine. An extensive review of the latest biomimetic and bioinspired materials and their application in engineering different tissues and organs has been collected by Jabbari et al. in the Handbook of Biomimetics and Bioinspiration series [10].

In the cornea, the bulk of the corneal ECM comprises type I collagen. However, our team had shown that recombinantly produced human type I and type III collagen behaved similarly as implants in mini-pigs over 12 months [11]. More importantly, we showed in a clinical study that carbodiimide crosslinked recombinant human collagen type III (RHCIII) hydrogels as corneal implants promoted epithelial and stromal cell and nerve regeneration [12]. Despite the successful regeneration, compression of the soft biomaterials by the sutures used in the surgery, as well as a sub-optimal fit into the wound bed, delayed epithelial coverage of the implant by endogenous in-growing epithelial cells, leading to localized implant thinning and fibrosis in some patients [12]. Hence, robust implants that could be grafted with more precision and without suturing, and that could encourage more rapid cell coverage to circumvent infection, would be a vast improvement for future clinical application. Indeed, others have shown that post-fabrication modification is often needed to ensure a seamless host–graft interface and/or modulate cell behaviour to obtain the desired clinical behaviour [13,14].

We have previously fabricated RHCIII implants that were reinforced by the introduction of a second network of 2-methacryloyloxyethyl phosphorylcholine (MPC) to form interpenetrating networks of RHCIII–MPC [15] and showed in a rabbit alkali burn cornea model of severe pathology that these hydrogels stimulated regeneration while repelling unwanted invasion of blood vessels into the implants [16]. In this study, we increased the mechanical strength of these hydrogels to render them suitable for post-fabrication modification to circumvent the problems of the previous generations of RHCIII and RHCIII–MPC implants. We evaluated the use of ultrahigh-speed femtosecond lasers developed for ophthalmic surgery to profile RHCIII–MPC hydrogels for surgical grafting. These lasers have been shown to produce cuts to within a 10 μm deviation from the target [17]. Creating matched cuts in the implant and surgical bed would allow precise lock-and-key fitting of the implant into host cornea, thereby enabling suture-free and hence compression-free retention. For surface modification to enhance cell attachment and rapid implant coverage, a range of established methods exist. These range from the creation of aligned collagen fibrils by molecular crowding [18] to various lithographic methods. However, most of these were developed for chips and other solid supports [19], but not for soft hydrogels that comprise over 85% water. Here, we tested the feasibility of microcontact printing (μCP) [20] as a means to introduce surface patterning onto fully hydrated, 500 μm thick hydrogels. Taking advantage of the improved mechanical stability of the RHCIII–MPC hydrogel, we printed and analysed micropatterns that used human fibronectin (FN) as "ink". FN is a cell-interactive protein in the ECM that promotes adhesion and migration of corneal epithelial cells during wound healing [21,22] and has been successfully tested therapeutically for the repair of persistent epithelial defects in human corneas [23]. We quantitatively evaluated the effect of the printed FN micropatterns on the growth of human corneal epithelial cells.

2. Materials and methods

2.1. Materials

All inorganic salts and basic chemicals were of analytical grade and purchased from Sigma–Aldrich (St. Louis, MO and Steinheim, Germany), Carl Roth GmbH (Karlsruhe, Germany) or Merck KGaA (Darmstadt, Germany) unless otherwise stated. Research grade RHCIII, produced in yeast (*Pishia pistoris*), was purchased from 3H Biomedical (Uppsala, Sweden) and FibroGen Inc. (San Francisco, CA). N-(3-Dimethylaminopropyl)-N′-ethylcarbodiimide (EDC), N-hydroxysuccinimide (NHS), 2-morpholinoethanesulfonic acid monohydrate (MES), poly(ethylene glycol) diacrylate (PEGDA, M_n = 575), ammonium persulphate (APS) and N,N,N,N-tetramethylethylenediamine (TEMED) were obtained from Sigma–Aldrich (MO, USA). MPC was obtained from Biocompatibles (UK) and Paramount Fine Chemicals Co. Ltd (Dalian, China).

2.2. Recombinant human collagen–phosphorylcholine hydrogels

RHCIII–MPC hydrogels were produced as previously published [15], but with a range of different starting concentrations of RHCIII to select the optimal formulation for laser profiling and μCP. Briefly, 450–500 mg of RHCIII solution of one of a range of starting concentrations (13.7, 18 or 20% (w/w)) was buffered with 150 μl of 0.625 M MES buffer within a syringe mixing system in an ice-water bath. Next, 200 μl of MPC solution in 0.625 M MES was added to the mixing system. The MPC:RHCIII (w/w) ratios used with either 1:4, 1:2 or 1:1. PEGDA was then added from a microsyringe (PEGDA:MPC (w/w) = 1:3). Calculated volumes of 4% (w/v) APS solution in MES and 2% (v/v) TEMED solution in MES were added sequentially (APS/MPC (w/w) = 0.015:1, APS:TEMED (w/w) 1:0.77). After thoroughly mixing, calculated amounts of NHS (10% (w/v) in MES) and EDC (5% (w/v) in MES) solutions were added and the reactants were thoroughly mixed at 0 °C (EDC: RHCIII–NH_2 (mol:mol) = 0.3–1.5:1, EDC:NHS (mol:mol) = 1:1). The final mixed solution was immediately cast into cornea-shaped moulds (12 mm diameter, 500 μm thick) or between two glass plates with 500 μm spacers. The hydrogels were cured overnight at 100% humidity under nitrogen at room temperature. The cornea-shaped implants were cured for an additional 5 h at 37 °C. After demoulding, they were washed thoroughly with 10 mM phosphate-buffered saline (PBS) and then stored in PBS containing 1% chloroform to maintain sterility.

2.3. Characterization of hydrogels

All samples were tested in triplicate. The water content of RHCIII–MPC hydrogels was determined by weighing samples that were blotted dry to remove surface liquid to obtain the wet weight (W_0). These pre-weighed hydrogels were then dried at room temperature under vacuum to constant weight, which is the dry weight (W). The equilibrated water content of hydrogels (W_t%) was obtained according to the following equation: $W_t\% = (W_0 - W)/W_0 \times 100\%$.

Optical properties of the resulting hydrogels were characterized by obtaining the refractive indices (RIs) of 500 μm flat, fully hydrated hydrogels equilibrated in PBS using an Abbe refractometer (Model C10, VEE GEE Scientific Inc., Kirkland, Washington) at 21 °C with bromonaphthalene as the calibration agent. Light transmission and backscattering measurements were carried out at 21 °C on a custom-built instrument equipped with a quartz halogen lamp for white light measurements, as previously reported [24]. The percentage light transmission through the hydrogels was compared to the open beam intensity. The amount of backscattered light (%) from each sample was measured by the circular array of eight built-in photodiodes, angled at 30° off axis.

The mechanical properties (tensile strength, moduli and elongation at break) were determined using an Instron mechanical universal tester (Model 3342, Instron, Canton, MA) equipped with a 10 N load cell and Instron Series IX/S software. Flat hydrogels (12 mm × 5 mm rectangular strips, 0.44 mm thick) were measured.

The gauge length of each specimen tested was 5 mm. The crosshead speed was 10 mm min^{-1} and the sampling rate was 10 points s^{-1}. Implants were not pre-stressed. Measurements were taken at room temperature.

The morphology of the RHCIII–MPC hydrogels compared to human corneas and RHCIII hydrogels alone was examined using scanning electron microscopy (SEM). All samples were lyophilized to minimize the shrinkage of the human cornea and collagen scaffolds due to the vacuum applied during freeze-drying and SEM imaging. Briefly, PBS-equilibrated samples of each construct or human eye bank corneas were frozen overnight at −80 °C and then placed in the drying chamber of a lyophilizer at a condenser temperature of −40 °C and vacuum pressure of 0.8, and dried for 7 h. The scaffolds did not collapse through the process, while there was some degree of shrinkage for all test samples, e.g. 40% for human cornea and 50% for the biosynthetic collagen hydrogels, due to the applied vacuum. The samples were then cut, using a sharp surgical knife, at a vertical angle to minimize the changes in the scaffolds' structure due to the cut, then attached to metal holders using conductive double-sided tape and sputter coated with a gold layer for 60 s at 0.1 bar vacuum pressure (Cressington Sputter Coater 108) prior to SEM examination. SEM micrographs were taken at 25 kV at various magnifications on a scanning electron microscope (Model S-2250N, Hitachi, Japan). Comparisons were made against human eye bank corneas prepared in the same way.

2.4. Precision laser cutting of the hydrogels and tissue welding

Laser trephination (or cutting) of three cornea-shaped RHCIII–MPC hydrogels (12 mm in diameter and 500 μm thick) was carried out using a femtosecond laser (IntraLase™ FS Laser, Abott Medical Optics, Abbott Park, Illinois, USA). The laser was set to cut out a top-hat-shaped implant from the hydrogel (one of the more common configurations for laser-assisted tissue trephination). The cutting parameters used were 6.0 mm diameter on the anterior side cut, 8.0 mm diameter on the posterior side cut and a depth of 250 μm for the lamellar cut. The energy used for the ring lamellar cut, anterior side cut and posterior side cut were 2.80, 1.50 and 1.50 μJ, respectively.

For implant/tissue welding, matched complementary cuts were also made on excised porcine corneas (obtained from an abbatoir) and RHCIII–MPC implants using a femtosecond laser (Wave Light GmbH Erlangen, Germany). RHCIII–MPC implants inserted into the matched donor cornea bed were welded together using standard riboflavin/dextran crosslinking techniques (1% riboflavin, 365 nm, 3 mW cm^{-2}, 30 min) [25] using a MLase UV crosslinking device (MLase AG, Germering, Germany).

2.5. Microcontact printing on hydrogels

RHCIII–MPC hydrogels containing 18% RHCIII, with RHCIII:MPC = 2:1 and EDC:RHCIII–NH_2 (mol:mol) = 0.4:1, were used for all μCP. Flat-cast hydrogels were cut into approximately 2 cm × 2 cm × 500 μm pieces and washed with 0.1 M PBS, pH 5.7, and dried under a nitrogen gas (N_2) stream prior to use. Free native carboxyl groups from the hydrogel surface were activated by immersing the samples in 2 ml of the PBS (pH 5.7) solution containing 10 mM EDC and 2.5 mM NHS for 15 min. All samples were rinsed for 30 s in fresh PBS buffer and dried with N_2 gas just before printing.

Square 1.5 cm × 1.5 cm poly(dimethylsiloxane) (PDMS; Dow Corning, Midland, MI, USA) stamps were prepared using a previously published protocol [26]. To examine the attachment and proliferation of single human corneal epithelial cells, a stamp comprising 30 μm wide protruding stripes separated by 60 μm spaces was designed. To examine the attachment and spread of multiple cells, 200 μm wide stripes, separated by 200 μm spaces, were tested. Prior to printing, the PDMS stamps were thoroughly rinsed in ethanol, dried under a stream of nitrogen gas and treated with oxygen plasma (20 W power) for 30 s in a plasma dry cleaner (Femto, Diener Electronic GmbH, Ebhausen, Germany). The stamps were then preloaded with "ink" comprising a 30 μl solution of 0.5 mg ml^{-1} human FN (Yo Proteins AB, Huddinge, Sweden) with 2 μg ml^{-1} bovine serum albumin conjugated with fluorescent Texas Red (BSA-TR®; Invitrogen, Eugene, OR, USA) in 0.1 M PBS buffer, pH 8.0, for visualization of the patterns. For cell seeding experiments, BSA-TR was omitted to avoid any unwanted nonspecific interactions between it and the cells. After 10 min of incubation with "ink" at room temperature, the stamps were rinsed in water for 20 s and dried for 1 min under a N_2 stream.

The activated RHCIII–MPC samples were placed in a Petri dish and then the upper surfaces were dried carefully with the N_2 gas in preparation for μCP. The bottom corners of the hydrogel samples were left in contact with water to prevent complete dehydration and therefore undesired deformation of the hydrogels. Surfaces were then printed by applying the PDMS stamp onto the hydrogel surface. All printing was performed manually without any load, using the nitrogen stream to bring the stamp into contact with the hydrogel surface. The stamp was left on for 5 min, then removed using tweezers. The patterned hydrogel surface was incubated with a solution containing 10 mM $(PEG)_3NH_2$ (Molecular Biosciences, Boulder, CO, USA) in PBS, pH 8.0, for 40 min to deactivate all remaining unreacted carboxyl groups. The surfaces were then carefully washed several times with fresh PBS, pH 7.3, and stored in this buffer solution prior to further use.

2.6. Characterization of printed hydrogels

To characterize the reproducibility of the μCP patterns, the optically transparent patterned hydrogels were imaged using an Olympus BX51 upright microscope (Olympus, Tokyo, Japan) equipped with a 10×, NA 0.3 water immersion objective and a Peltier-cooled Fview II CCD camera (Olympus Soft Imaging Solutions GmbH, Münster, Germany). Fluorescence images of fibronectin–BSA-TR® patterns were acquired and analysed using analySIS software (Olympus Soft Imaging Solutions GmbH, Münster, Germany).

The presence of FN in the micropatterns was confirmed by using a primary rabbit polyclonal antibody against FN (Abcam, Cambridge, UK), followed by a secondary antibody, donkey anti-rabbit IgG, conjugated with quantum dots Qdot655 (H+L) (Life Technologies, USA).

To investigate the effect of μCP on the micro- and nanotopography of fully hydrated RHCIII–MPC constructs, atomic force microscopy (AFM) measurements were carried out with the samples fully immersed in 0.1 M PBS buffer, pH 7.3, using a NanoWizard® 3 AFM microscope (JPK Instruments AG, Berlin, Germany) mounted onto an Olympus IX81 inverted optical microscope (Olympus, Tokyo, Japan) to allow for combined optical and AFM imaging of the same surface. Sample topography images were obtained in contact mode using SNL-10 probes (Bruker, Billerica, MA, USA). Regions of interest for AFM analysis were selected with fluorescence microscopy to include the printed and unprinted zones of the surface within one large area (70 × 70 μm^2) scan. Several different size scans were made. Images obtained were processed and the surface roughness was calculated using the region analysis tool within the AFM JPK data processing software.

2.7. Cytotoxicity evaluation

All samples with 30 and 200 μm patterned stripes, and control samples comprising deactivated and unmodified hydrogels, were

placed into 24-well plates. Immortalized human corneal epithelial cells (HCECs) [27] were seeded onto the surface of the materials at a density of 2×10^4 cells per well. The HCECs were maintained in keratinocyte serum-free medium (KSFM; Life Technologies, Invitrogen, Paisley, UK) containing 50 μg ml^{-1} bovine pituitary extract and 5 ng ml^{-1} epidermal growth factor for 48 h in a humidified 37 °C incubator. Cell viability was measured by using a Live/Dead staining kit (Life Technologies, Invitrogen, Paisley, UK), where cells were double-stained by calceinacetoxymethyl (Calcein AM) and ethidium homodimer-1 (EthD-1). The live cells displayed green fluorescence, while the dead cells fluoresced red.

2.8. Cell attachment and proliferation

Green fluorescence protein (GFP) transfected HCECs were employed to facilitate cell counts. A stable GFP-HCEC cell line was established by the transfection of HCEC cells with a vector containing a puromycin-resistant gene together with GFP, using the Lipofectamine® 2000 Transfection Reagent (Life Technologies, California, USA). Selection of puromycin-resistant cells with 2 μg ml^{-1} of puromycin added to the medium was performed to obtain stable GFP-expressing lines.

To examine proliferation rates on the different surfaces, 6 mm hydrogel discs with 30 and 200 μm FN striped patterns, and PEG-NH_2 deactivated and unmodified samples, were fitted snugly into 96-well plates. Five thousand GFP-HCECs were seeded into each well. GFP-HCECs were also seeded onto the tissue culture plate as a control for overall cell health. The cells were maintained in KSFM within a humidified 37 °C incubator with 5% CO_2. Photomicrographs of the cells were taken at 2, 6, 24, 48 and 96 h, using a fluorescence microscope (AxioVert A1, Carl Zeiss, Göttingen, Germany). Counts were made by sampling three different 1290 × 965 μm^2 areas on each hydrogel surface.

2.9. Immunohistochemistry

GFP-HCECs were cultured on hydrogels for 4 days, by which time the cells had reached confluence/near confluence on the patterns. Each sample was washed in 10 mM PBS, pH 7.4, then fixed in 4% paraformaldehyde in PBS for 20 min. For permeabilization and blocking of unspecific binding, samples were incubated in PBS containing 0.25% Triton X-100 for 10 min and 5% foetal calf serum (FCS) in PBST (0.05% Tween-20 in PBS) (FCS/PBST) for 1 h, respectively. Samples were then incubated overnight at 4 °C with the following primary antibodies diluted in FCS/PBST: anti-proliferating cell protein Ki67 antibody (1:600; Sigma–Aldrich, MO, USA), anti-focal adhesion kinase (FAK) antibody (1:500; Abcam, Cambridge, UK) and anti-integrin beta 1 (integrin β1) antibody (1:200; Abcam). After rinsing, the samples were exposed to the secondary antibody, Alexa Fluor-594 (1:400; Invitrogen, Oregon, USA) at room temperature for 1 h in the dark for visualization. After another rinse, the samples were incubated with 4′, 6-diamidino-2-phenylindole dihydrochloride (PromoKine, Heidelberg, Germany) for 1 min as a nuclear counterstain. All samples were given a final rinse prior to mounting and examination under a confocal microscope (LSM700, Carl Zeiss, Göttingen, Germany). A total area of 50,000 μm^2 per sample was used for all the counts.

2.10. Statistical analyses

Statistical analyses were performed using general linear models that relate responses to linear combinations of predictor variables. These *p* value tests were followed by a Tukey test in cases where significance was found. The analyses were performed using Minitab© software (Minitab Ltd., Coventry, UK). Ratios of cell populations are shown in Fig. 5 as percentages and are therefore not portrayed with standard deviations. The ratio data have skewed distributions that are close to zero and one. Hence, these data were log transformed before analysis to better comply with the assumptions of general linear models. Intervals for feature sizes are ±1 standard deviation.

3. Results

3.1. RHCIII–MPC hydrogels

A range of adjustments in hydrogel formulations were tested for producing a mechanically reinforced material suitable for post-fabrication of the implants. These included starting RHCIII contents of 13.7, 18 and 20%, and different RHC:MPC and EDC:RHCIII–NH_2 ratios. The resulting optical and mechanical properties of the hydrogels are given in Appendix A. The resulting enhancement in properties of RHCIII–MPC hydrogels after optimization of the above parameters as compared to our previously published formulation [15] is shown in Table 1. In both the 13.7 and 18% RHCIII–MPC hydrogels, we found that a 2:1 RHCIII:MPC ratio with 0.4:1 EDC:RHCIII–NH_2 gave the optimal formulations.

Increasing the collagen content from 13.7 to 18% decreased the water content from 90.1 ± 2.4 to approx. 86% (85.5 ± 0.2% for RHCIII–MPC and 86.0 ± 0.2% for RHCIII only). Thus, the MPC content did not make much of a difference. Additionally, the EDC:RHCIII–NH_2 ratio showed no obvious influence on the RI, while the RI increased with increasing MPC content within the gels.

Table 1
Comparison of key properties of 18% RHCIII–MPC (RHCIII:MPC (w/w) = 2:1; EDC:RHCIII–NH_2 (mol:mol) = 0.4:1) hydrogels with a previous 13.7% RHCIII–MPC (RHCIII:MPC (w/w) = 2:1; EDC:RHCIII–NH_2 (mol:mol) = 0.3:1) hydrogel formulation grafted onto alkali burn rabbit cornea and 18% RHCIII-only (EDC:RHCIII–NH_2 (mol:mol) = 0.4:1) hydrogels, with human cornea properties from the literature serving as a benchmark.

Properties	13.7% RHCIII–MPC*	18% RHCIII–MPC	RHCIII only	Human cornea
Water content (%)	90.1 ± 2.4	85.5 ± 0.2	86.0 ± 0.2	78 [40]
Optical properties:				
Refractive index	1.35	1.36	1.35	1.37–1.38 [28]
Transmission (%)	98.3 ± 1.5	91.6 ± 0.46	87.4 ± 0.9	87 [41]
Backscatter (%)	1.8 ± 0.0	1.9 ± 0.2	1.3 ± 0.4	3 [42]
Mechanical properties:				
Tensile strength (MPa)	1.29 ± 0.31	2.12 ± 0.18	2.37 ± 0.4	3.81 ± 0.4 [43]
Elongation at break (%)	37.89 ± 10.31	33.34 ± 3.87	28.21 ± 2.01	
Elastic modulus (MPa)	5.26 ± 1.5	9.46 ± 3.58	15.33 ± 2.67	3–13 [44,45]
Thermodynamic properties:				
Td (°C)	54.1	57.6	53.1	65.1 [11]

* Data from [15].

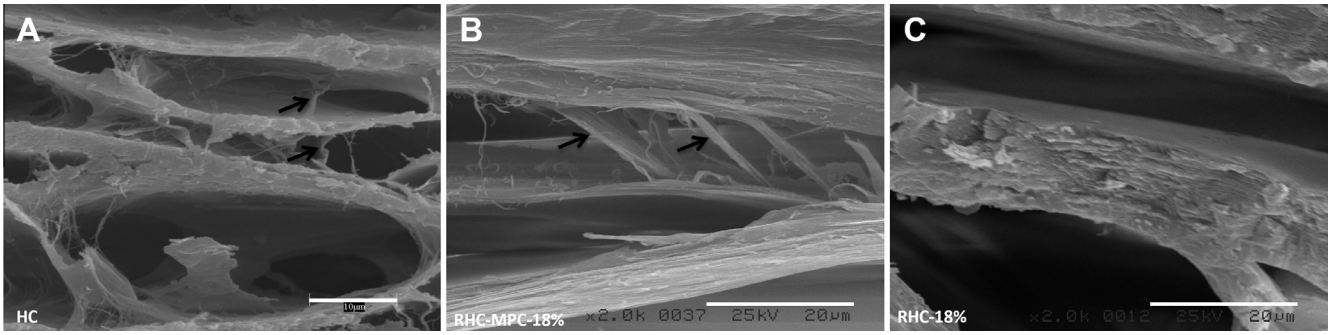

Fig. 1. SEM micrographs of cross-sections of (A) human cornea, showing the lamellar structure of the collagenous ECM with inter-lamellar connections (arrows) (scale bar, 10 μm); (B) 18% RHCIII–MPC(2/1) hydrogel crosslinked with EDC (RHCIII:MPC (w:w) = 2:1 and EDC:RHCIII–NH_2 (mol:mol) = 0.4:1), showing lamellae and inter-lamellar connections; and (C) 18% RHCIII-only hydrogel crosslinked with EDC (EDC:RHCIII–NH_2 (mol:mol) = 0.4:1), depicting the lamellar structure without the inter-lamellar connections (scale bars, 20 μm).

The measured transmittance of white light decreased with the increased RHCIII concentration. Compared to the native cornea (transmittance: ~87%; backscatter: ~3%), however, all the RHCIII–MPC gels showed a higher transmittance and lower backscatter. The RHCIII-only gels, on the other hand, exhibited a transmittance comparable to the native cornea (approx. 87%). All the cornea substitutes displayed a slightly lower RI of 1.35, which is that of water, compared to native cornea (1.37–1.38 [28]).

The effect of the material composition on mechanical properties is summarized in Fig. A2 (Appendix A). In general, increasing the solids content of the hydrogels from 13.7 to 18% increased the tensile strength of RHCIII–MPC hydrogels from 1.29 ± 0.31 to 2.12 ± 0.18 MPa (Table 1). The tensile strengths of the 18% RHCIII-only hydrogels were comparable to the 18% RHCIII–MPC hydrogels, at 2.37 ± 0.4 MPa. However, the RHCIII-only hydrogels were stiffer (an elastic modulus of 15.33 ± 2.67 MPa) and less elastic (elongation at break of 28.21 ± 2.01%) than the corresponding RHCIII–MPC hydrogels (lower elastic modulus of 9.46 ± 3.58 MPa; higher elongation at break of 33.34 ± 3.87%).

The 18% RHCIII–MPC hydrogels were more thermodynamically stable (Td = 57.6 °C) than both the 18% RHCIII-only (Td = 53.1 °C) or 13.7% RHCIII–MPC hydrogels (Td = 54.1 °C). However, none were as stable as the native corneas (Td = 65.1 °C) (Table 1).

SEM imaging of cross-section of samples was performed for structural comparison of the produced RHCIII–MPC and RHCIII-only hydrogels with native human corneas. A distinct lamellar structure could be seen for both human and biosynthetic corneas (Fig. 1A–C). The lamellar structure was observed throughout the entire cross-section of all samples, while it was more homogeneous for the human cornea and better representative of the whole structure than that of the biosynthetic ones. In addition, the RHCIII–MPC hydrogels comprised lamellae-like layers interconnected by some tiny fiber-like structures (Fig. 1B), which better mimics the structure of the human cornea (Fig. 1A) than the RHCIII crosslinked by EDC/NHS, which had large lamellae without any inter-lamellar connections (Fig. 1C). However, the inner morphology of the biosynthetic corneas differed from that of their native counterpart in the number of lamellar layers and the spacing between layers. For example, the lamella-like layers in the biosynthetic corneas were thicker and fewer compared to the lamellae of the native cornea. In addition, the spacing between the ordered lattice structures of the native cornea was smaller (~15 μm) than that of the biosynthetic corneas (~150 μm). The lamellar spacing for the human cornea had a wide size distribution ranging from 2 to 40 μm. Overall, despite some similarities between the biosynthetic corneas and their natural counterparts, the human cornea has a much more complex microstructure with a higher degree of interconnectivity, as expected.

3.2. Precision laser profiling and tissue welding

The optimized hydrogels were sufficiently robust to allow complete cutting of "top-hat" implants using the femtosecond laser. The resulting mean dimensions of the cuts were an anterior diameter of 5.9 mm, a posterior diameter of 8.1 mm and a depth of 260 μm for the lamellar cut (Fig. 2A). For example, RHCIII–MPC hydrogels containing 18% RHCIII, with RHCIII:MPC = 2:1 and EDC:RHCIII–NH_2 (mol:mol) = 0.4:1 (designated RHCIII-18/MPC(2/1)-E0.4), which had shown good mechanical properties, cut well with the laser. As shown in Fig. 2B, top-hat-shaped gels with precisely cut edges could be obtained. However, hydrogels with the lower 13.7% RHCIII content (but otherwise with the same proportions of MPC and EDC crosslinker) fell apart during cutting (data not shown).

Laser-cut implants were successfully fitted into matched laser-cut surgical beds (Fig. 2C). After riboflavin/UV crosslinking, the implants remained permanently adhered to the corneal bed (Fig. 2D), and submicroscopic physical fibre-like connections were present between the implant and adjacent cornea (Fig. 2E) when viewed by SEM. In contrast, implants detached completely in controls without UV irradiation.

3.3. Overall quality of the microcontact printed patterns

The most stable RHCIII-18/MPC(2/1)-E0.4 hydrogels that lent themselves well to laser profiling were also optimal for μCP (process diagramed in Fig. 3A). Fig. 3B and C show the typical resulting striped FN patterns, as visualized by staining with an anti-fibronectin antibody. Analysis of the fluorescence micrographs of the hydrogel samples confirmed good replication of the original patterns of the 30 and 200 μm stripes defined in the photolithographic mask production step (not shown). On the PDMS stamp, the width of the narrow stripes was 26.8 ± 0.5 μm (based on bright-field microscopy), while that of the printed FN stripes was 27.1 ± 0.8 μm. The thick stripes on the PDMS stamps and the resulting FN patterns had widths of 190.6 ± 1.7 and 191.7 ± 2.6 μm, respectively. The good reproducibility indicated that uncontrolled FN ink diffusion on partially dried collagen hydrogel samples was minimal. On the samples printed with the 30 μm stripe pattern, the printed area occupied approx. 37% of the sample area, and approx. 32% of the total hydrogel surface was patterned and defect-free. On the 200 μm striped samples, the printed sample area occupied 40% of the sample, and approx. 26% of the total hydrogel surface was printed and free from printing defects. Also, FN ink distribution on the entire patterned surface was satisfactorily homogeneous.

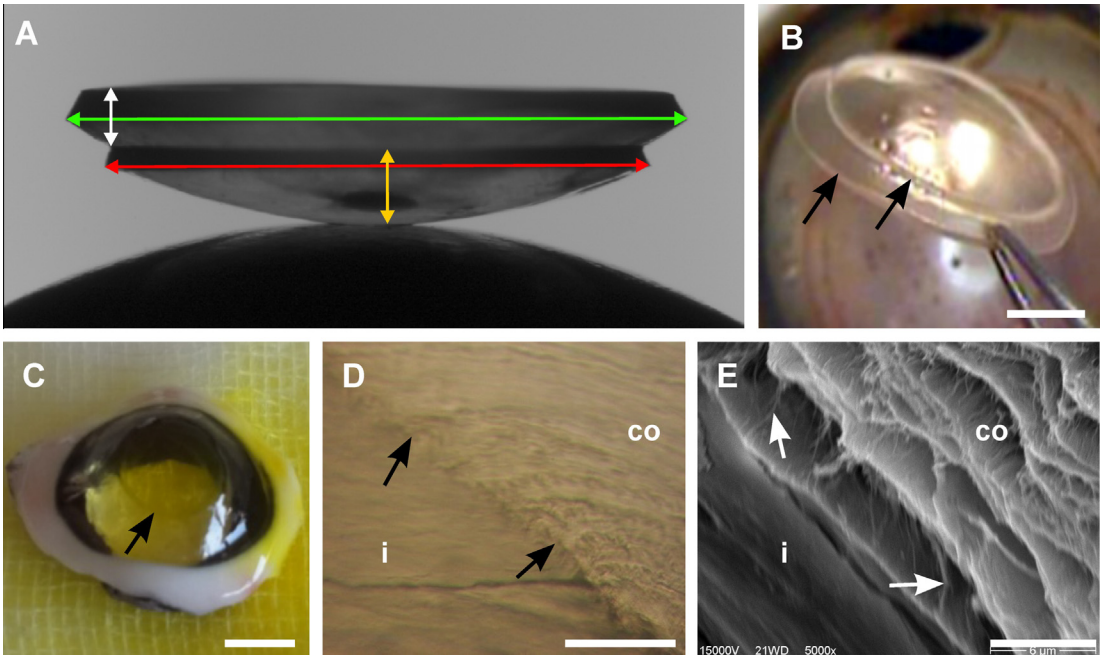

Fig. 2. (A) RHCIII–MPC implant after cutting with a femtosecond laser, showing the dimensions of the cuts. Red arrow: anterior diameter of 5.9 mm; green arrow: posterior diameter of 8.1 mm; yellow arrow: anterior lamellar cut of 260 μm; white arrow: remaining posterior depth of 240 μm. (B) Laser-cut implant forming a top-hat-shaped hydrogel. The precisely cut edges are indicated by arrows. Scale bar, 2 mm. (C) Cut implant after tissue welding to a matched laser-cut surgical bed in an excised pig cornea by UV crosslinking. The apposed edges are arrowed. Scale bar, 4 mm. (D) Cornea (co) and implant (i) as viewed under polarized light, showing the very tight apposition between the implant and host tissue after tissue welding (arrows). Scale bar, 50 μm. (E) SEM image of the "welded" implant–cornea interface, showing the presence of small fibrous crosslinks (arrows) established between the two. Scale bar, 6 μm.

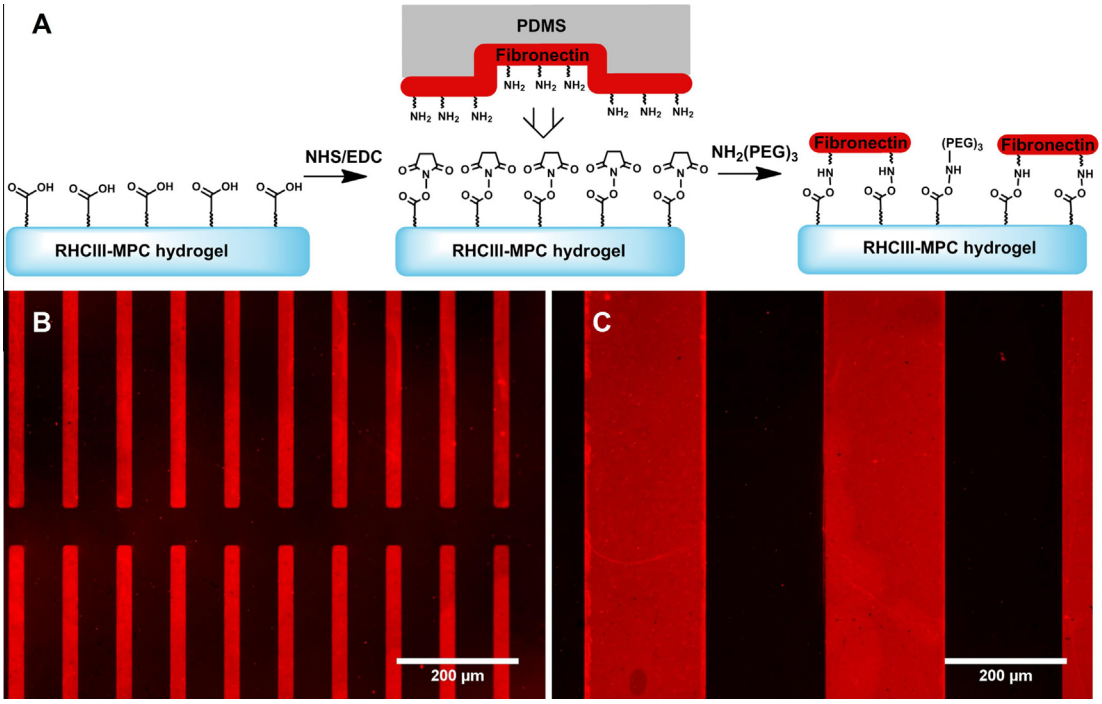

Fig. 3. (A) Schematic of the microcontact printing procedure, including free collagen hydrogel carboxyl group activation, "ink" printing and passivation steps. Fluorescence microscopical images of the resulting patterned (B) 30 μm and (C) 200 μm stripes on the surface of RHCIII–MPC hydrogels, visualized by staining with an anti-fibronectin antibody.

3.4. Atomic force microscopy

The effect of μCP on the micro- and nanotopography of fully hydrated RHCIII–MPC hydrogels was determined by AFM analysis. The original, unmodified collagen hydrogel surfaces appeared uneven, with irregularly arranged surface fibrils visible (Fig. 4A). The root mean square (RMS) of surface roughness as measured within a representative $2 \times 2\ \mu m^2$ scan area was 3.5 nm. The regions of interest (ROIs) for AFM scans on the chemically activated and microcontact printed samples were identified by simultaneous

fluorescence microscopy imaging. The AFM tip was positioned in the ROIs that were patterned with FN and BSA-TR® mixture. In topography images of the hydrogel surface after μCP and/or deactivation, the collagen fibrils appeared to be partially aligned (Fig. 4B), in contrast to the unmodified surface (Fig. 4A). However, the fine details of the collagen fibrils could not be resolved. There was no distinct overall height difference between the majority of the printed and adjacent unprinted areas, due either to the high initial surface roughness and/or the ability to print a very thin, possibly monolayer, thickness of FN. The edges of the stripes, however, were slightly corrugated by the printing and served to delineate the stripe boundaries. The RMS surface roughnesses of the FN-printed and unprinted regions on this particular sample shown in Fig. 4B were very similar, at 1.3 and 1.4 nm, respectively. The AFM analysis therefore showed that the μCP resulted only in a very small change in the surface topology.

3.5. Effect of patterning on cytotoxicity, cell adhesion and proliferation

Printing with PDMS stamps can result in a slight contamination of the sample surface with loose PDMS particles [26,29], but these can be removed by subsequent sample deactivation and washing steps. The Live/Dead staining performed showed that there were no cytotoxic effects from the patterning. The numbers of dead cells (stained red) were negligible: 0 in most of the samples, 1–2 cells in a few others (Fig. 5A–D).

Analysis of the proliferation of HCECs on the different surfaces over time showed obvious differences between the patterned and non-patterned samples (Fig. 5E). The only two types where the growth rate could not be told apart ($p > 0.05$) were the unmodified and deactivated RHCIII–MPC surfaces. The total number of cells counted per defined ROI was highest on the hydrogels patterned with 200 μm stripes. However, when taking into account that the total FN-coated surface area per ROI on the 30 μm pattern was half that on the 200 μm pattern, the results show that the thinner stripes yielded approx. 26% more cells after normalization of the surface areas.

3.6. Immunohistochemistry and cell behaviour

Fig. 6 shows the behaviour of cells on the different surfaces. The integrin β1 family, which is involved in binding ECM macromolecules, including collagen and FN, was expressed by HCECs growing on all groups. The proportions of integrin β1-expressing cells in the deactivated surfaces and the 30 and 200 μm patterns were significantly different from those growing on the unmodified RHCIII–MPC hydrogel surfaces (Fig. 6A), with the highest expression on the 30 μm stripes, although this was not significantly different from the 200 μm stripes or the deactivated surfaces ($p > 0.05$).

Immunohistochemical localization of FAK-positive cells showed that significantly more cells were growing on the 30 μm striped patterns that were positively stained ($p \leqslant 0.05$) than those of the other groups (Fig. 6B).

Staining for the Ki67 protein associated with cell proliferation showed that the samples with 30 μm striped patterns supported a significantly larger proportion ($p \leqslant 0.05$) of positively stained cells than the other groups (Fig. 6C).

4. Discussion

Hydrated interpenetrating networks of RHCIII–MPC hybrid hydrogels were prepared by simultaneous crosslinking of RHCIII with EDC/NHS and radical polymerization of MPC monomer with APS/TEMED as the initiator system and the PEGDA as the macromolecular crosslinker. Biphasic responses were found in hydrogels with increases in RHCIII starting concentration and MPC content. In particular, the increased MPC content that ensued in RHCIII:MPC molar ratios of 1:1 resulted in weak, brittle hydrogels. This could be due to the high MPC concentration, which might have hindered the entanglement and crosslinking of the RHCIII microfibrils. The increased RHCIII concentration from 18 to 20%, which resulted in overall weaker gels, could be due to the increase in viscosity of the collagenous mixture making it difficult to properly crosslink the very viscous RHCIII. The higher solids content would therefore have made the hydrogel stiffer but not stronger. An increase in EDC concentration relative to RHCIII–NH_2 content beyond 0.4 did not enhance the strength of the hydrogels. The combination of 18% RHCIII with an RHCIII:MPC ratio of 2:1 and a molar equivalent of 0.4 EDC (RHCIII-18/MPC(2/1)-E0.4) resulted in strong, stable and optically clear hydrogels. Although they comprised over 85% water, these hydrogels were nevertheless sufficiently robust for subsequent post-fabrication modifications, i.e. laser cuts and μCP.

SEM analysis shows that both RHCIII-only and RHCIII–MPC hydrogels had a lamellar arrangement of collagen fibrils. The addition of the second network resulted in additional fibrous structures that connected the lamellae in RHCIII–MPC hydrogels.

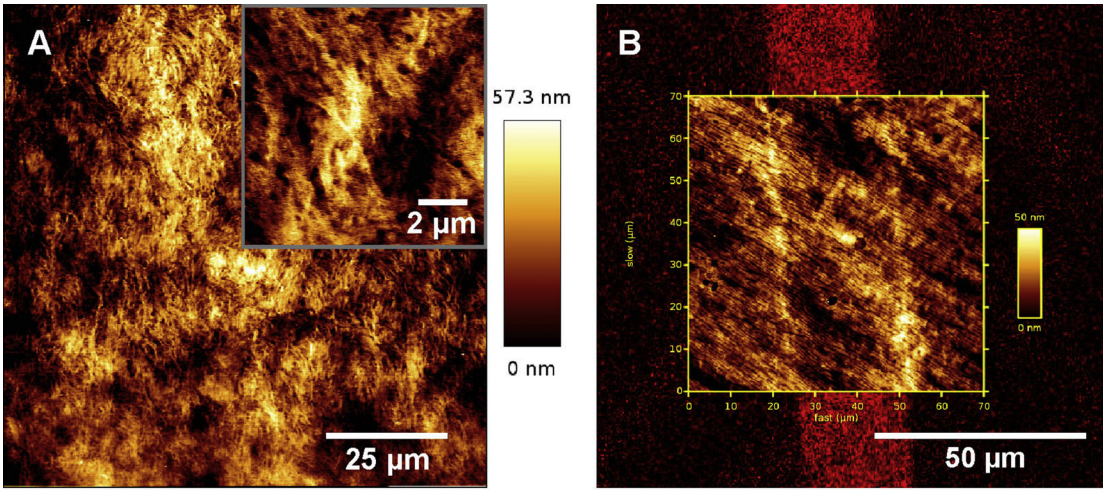

Fig. 4. Contact mode AFM topography images of the RHCIII–MPC hydrogel surface before and after the microcontact printing. (A) Unmodified hydrogel, showing a surface that comprised uneven, irregularly arranged fibrils. Inset, 10 μm scan image. (B) Printed hydrogel surface, overlaid with a fluorescence microscopy image of a printed fibronectin stripe. Surface collagen fibrils that were visible appeared to be partially aligned.

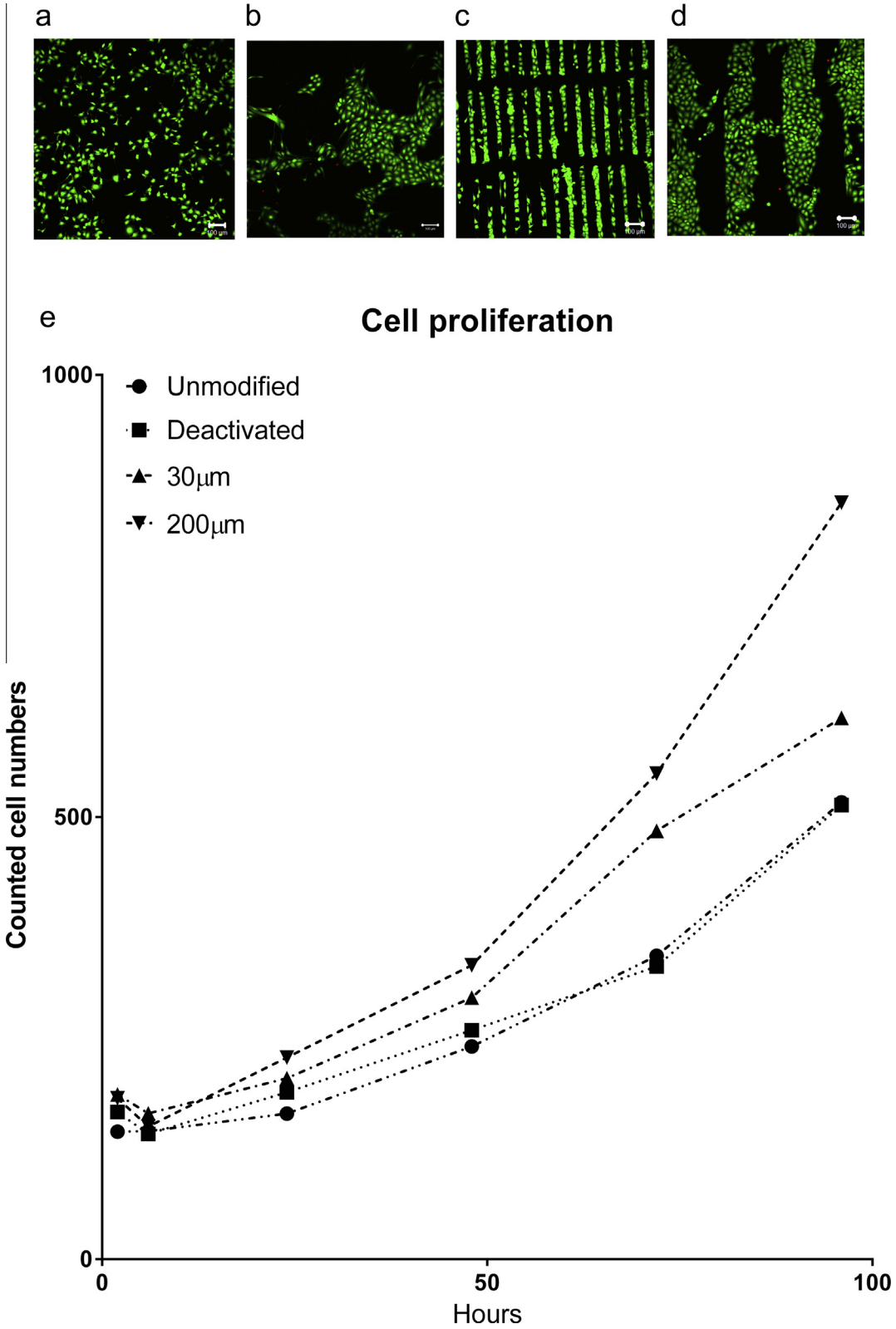

Fig. 5. Cell growth on RHCIII–MPC hydrogel surfaces that were (A) unmodified, (B) deactivated, or patterned with (C) 30 μm and (D) 200 μm lines. Live/Dead staining shows live cells as green, while dead cells fluoresce red. Scale bars, 50 μm. The proliferation rate of cells on the different surfaces is shown in (E).

These tiny inter-lamellar structures were only seen in the RHCIII–MPC hydrogels, and were likely the result of combined long-range and short-range crosslinkers that resulted in an interpenetrating network. The inter-lamellar connecting structure was not observed in RHCIII-only scaffolds. Nevertheless, the interconnected multilayer structure was simpler and sparser than that of the native corneas, which had a larger number of lamellae and many more inter-lamellar connections. The driving force

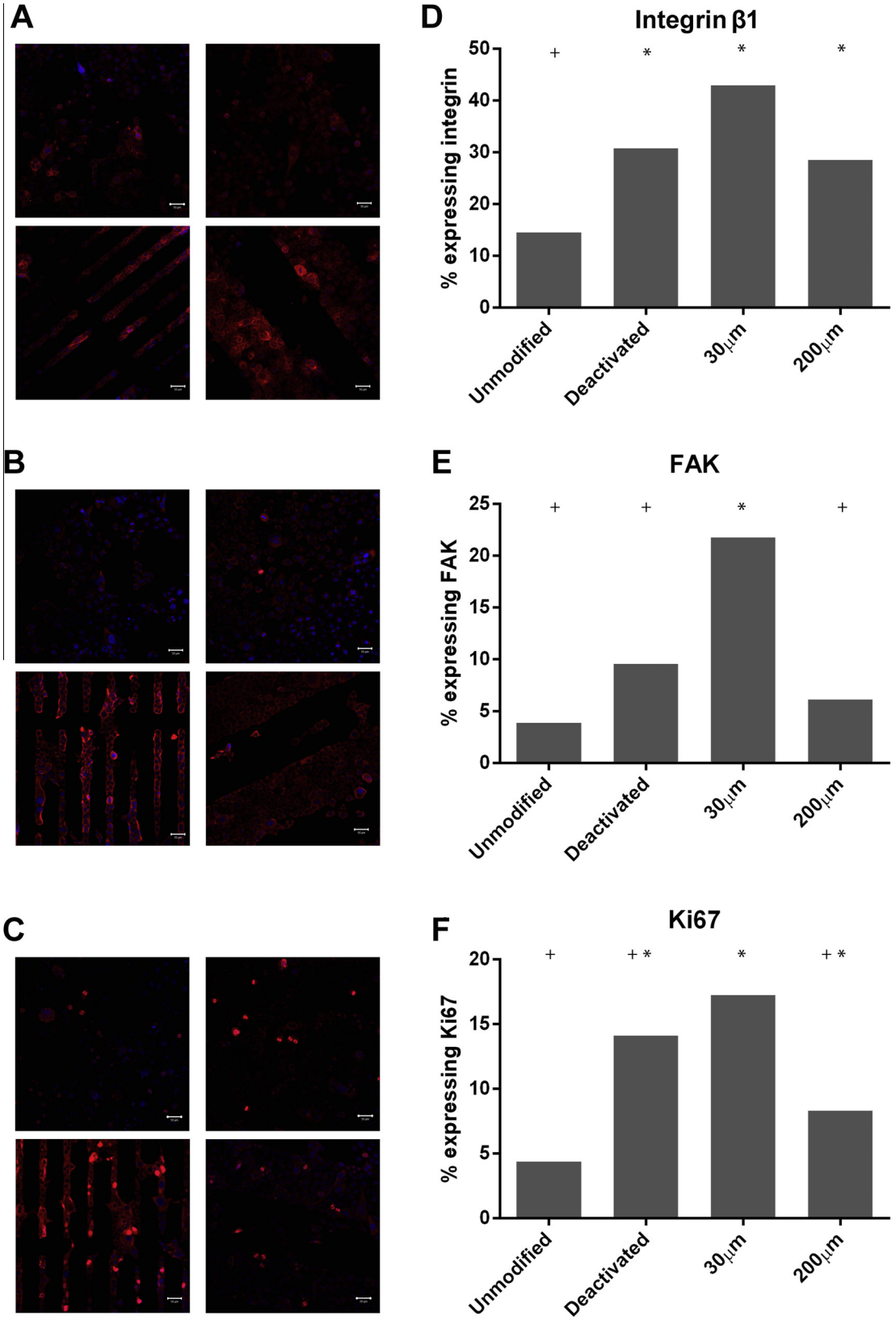

Fig. 6. Immunostaining for (A) integrin β1, (B) FAK and (C) Ki67. The micrographs show cells on the hydrogel surfaces, from top left – deactivated, top right – unmodified, bottom left – patterned 30 μm stripes and bottom right – patterned 200 μm stripes. Scale bars, 50 μm. The bar graphs show the ratios between the total cell count and the cells stained for (D) integrin β1, (E) FAK and (F) Ki67. Bars with similar symbols (* or +) are not significantly different from each other ($p > 0.05$ by Tukey test). In contrast, bars with dissimilar symbols are significantly different ($p \leqslant 0.05$) from each other.

behind the formation of the lamellar structures is unclear. The most plausible explanation has been put forward by Ruberti's group [18,30]. At the high collagen concentrations used to fabricate implants and under the confined environment of the moulds used, molecular crowding as described by Ruberti et al. is present. Prior to moulding, the collagen is mixed very thoroughly using a syringe mixing system [31], which generates a lot of shear force. During the moulding, the mixed collagen is then compressed within the mould with a final compression-cum-shearing action.

Femtosecond lasers are now being used in surgery, particularly ophthalmic refractive surgery, as alternatives to conventional mechanical cutting tools. They have ultrashort (10^{-15} s) pulses that can cut out three-dimensional shapes within the cornea by producing multiple adjacent minute spots of explosions in it. The RHCIII-18/MPC(2/1)-E0.4 hydrogels, like human corneal tissue, lent themselves to being precisely cut by the femtosecond laser, as shown by the resulting well-defined cuts. In contrast, the laser pulses broke up weaker hydrogels. This shows that RHCIII–MPC hydrogels were sufficiently robust to maintain their integrity during the laser cutting, which is important for grafting applications without sutures. We also showed that, in the excised porcine corneas, the implants could be precisely fitted and welded together with the host cornea. This opens up the possibility of future sutureless implantation, or the use of fewer sutures.

Microcontact printing has been used as a method to transfer proteins and other biological macromolecules onto solid substrates without the loss of their biological activity [32,33]. However, most of the literature on μCP applications typically describes patterning on hard substrates such as glass, silicon, metals or robust and elastic polymers (e.g. polystyrene, polymethylmethacrylate, PDMS) [32–34]. In this study, we showed that μCP could be used to introduce reproducible functional protein patterns onto the surfaces of thick, highly hydrated, largely collagenous matrices. The reproducibility of the patterns was good, with a standard deviation of 0.8 μm for the 30 μm pattern and 2.6 μm for the 200 μm pattern. It should be noted that the RHCIII–MPC hydrogels developed in this study for μCP had a tensile strength of 2.15 ± 0.14 MPa and an elastic modulus of 10.53 ± 3.25 MPa. This is comparable to the 2.24 MPa tensile strength and elastic modulus of 0.360–0.870 MPa for PDMS [35], which is a common stamp material used for μCP. However, unlike PDMS, which is hydrophobic, the RHCIII–MPC hydrogels comprised 85.5 ± 0.2% water.

Fibronectin is a large glycoprotein that is present in the basement membrane of the normal corneal epithelium. Its elaboration is increased during wound healing and the macromolecule appears at wound sites, where it serves as a temporary matrix for cell migration [36]. The fibronectin molecule and its bioactive peptide derivatives Arg–Gly–Asp (RGD) and Pro–His–Ser–Arg–Asn (PHSRN) have been reported to enhance healing of corneal epithelial wounds in rabbit models [21,22] and in clinical trials [23]. Fibronectin enhances wound healing through its interactions with β1 integrins. Corneal epithelial cells express β1 integrins and migrate over the newly laid down FN. After healing is complete, the expression of both integrin and FN is diminished [36].

Cell attachment to FN triggers integrin-mediated signalling. Previously, β1 integrin–FAK signalling has been shown to initiate proliferation of metastatic lung cancer cells [37] and other cell types, for example, in this case, HCECs. In our hydrogels, there was a trend towards the aligned cells on 30 μm FN stripes having the highest expression of β1 integrin, FAK and Ki67, showing that the width of the patterned FN stripes was able to influence cell behaviour. Thus, although the total number of the cells counted per ROI was highest on the 200 μm stripe pattern, proliferation as demonstrated by the expression Ki67, a cellular marker for proliferation, was highest in the 30 μm stripes. We have therefore shown that, despite the ability of the unmodified RHCIII–MPC hydrogels to support corneal epithelial cells, the attractiveness of the hydrogel as a substrate was enhanced by the transfer of FN onto the hydrogel surface. Micropatterning has been previously used to manipulate cell growth and differentiation, and nanoscale topography has been shown to affect corneal epithelial cell migration [38]. In the present study, however, there was little change in pitch, and the surface roughnesses of the printed and unprinted areas were similar. The manipulation of cell adhesion has been found to affect mitosis [39]. In our study, the 30 μm stripes are approximately the diameter of a corneal epithelial cell, so each cell will only have two neighbours along the FN stripe. On the 200 μm stripes, each cell is surrounded by neighbouring cells. It would appear that a combination of the differential adhesion afforded by the FN and the presence/absence of neighbouring cells affected the proliferation of corneal epithelial cells on our surfaces. Whether or not the micropatterning with an array of thin stripes that promoted the highest proliferation rates will do the same in vivo is yet to be determined by micropatterning on cornea-shaped hydrogels for animal studies.

5. Conclusion

We have shown that biomimetic hydrogels comprising interpenetrating networks of synthetically produced human collagen and phosphorylcholine can attain mechanical properties that are suitable for post-fabrication modification using laser cutting and μCP. Use of the femtosecond laser produced highly precise cuts on the RHCIII–MPC gels that would be suitable for implantation. Microcontact printing of FN was able to further enhance cell adhesion and growth on the 500 μm thick, already biocompatible hydrogels that comprised over 85% water.

Acknowledgements

We thank Dr. Chyan-Jang Lee for establishing the GFP-HCEC cell line used for this study, and Ms. Kimberley Merrett for assistance in characterization of the hydrogels. We also thank Dr. Sadhana Kulkani and David Priest, University of Ottawa Eye Institue, for assistance with the laser cutting study; and Dr. Joanne M. Hackett (currently at Cambridge University Health Partners) for assistance with preliminary cell culture/biocompatibility studies during optimization of the RHCIII–MPC hydrogels. We thank Johannes Junger and Michael Baumann, MLase AG, for help with the UV crosslinking, and the Medical Devices Bureau, Health Canada, for use of the SEM system. We gratefully acknowledge funding from an NSERC-CIHR Canada Collaborative Health Research Project grant (M.G.) and subsequent funding for an EU Nanomedicine ERAnet project "I-CARE" to M.G., R.V. and MLase AG, through the Swedish Research Council, Research Council of Lithuania and VDI Germany, respectively.

Appendix A. Figures with essential colour discrimination

Certain figures in this article, particularly Figs. 3, 4, 6 are difficult to interpret in black and white. The full colour images can be found in the on-line version, at http://dx.doi.org/10.1016/j.actbio.2014.10.035.

Appendix B. Supplementary data

Supplementary data associated with this article can be found, in the online version, at http://dx.doi.org/10.1016/j.actbio.2014.10.035.

References

[1] Fink J, Thery M, Azioune A, Dupont R, Chatelain F, Bornens M, et al. Comparative study and improvement of current cell micro-patterning techniques. Lab Chip 2007;7:672–80.
[2] Chung BG, Lee KH, Khademhosseini A, Lee SH. Microfluidic fabrication of microengineered hydrogels and their application in tissue engineering. Lab Chip 2012;12:45–59.
[3] Thevenot P, Hu W, Tang L. Surface chemistry influences implant biocompatibility. Curr Top Med Chem 2008;8:270–80.
[4] Jeon HJ, Simon CG, Kim GH. A mini-review: cell response to microscale, nanoscale, and heirarchical patterning of surface structure. J Biomed Mater Res B Appl Biomater 2014;00B.
[5] Singh RK, Seliktar D, Putnam AJ. Capillary morphogenesis in PEG–collagen hydrogels. Biomaterials 2013;34:9331–40.
[6] Hynd MR, Frampton JP, Dowell-Mesfin N, Turner JN, Shain W. Directed cell growth on protein-functionalized hydrogel surfaces. J Neurosci Methods 2007;162:255–63.
[7] Klenkler BJ, Griffith M, Becerril C, West-Mays JA, Sheardown H. EGF-grafted PDMS surfaces in artificial cornea applications. Biomaterials 2005;26:7286–96.
[8] Lim JY, Donahue HJ. Cell sensing and response to micro- and nanostructured surfaces produced by chemical and topographic patterning. Tissue Eng 2007;13:1879–91.
[9] Coq N, van Bommel T, Hikmet RA, Stapert HR, Dittmer WU. Self-supporting hydrogel stamps for the microcontact printing of proteins. Langmuir 2007;23:5154–60.
[10] Jabbari E, Kim DH, Lee LP, Ghaemmaghami A, Khademhosseini A, editors. Biologically-Driven Engineering of Materials, Processes, Devices, and Systems. Handbook of Biomimetics and Bioinspiration. Singapore: World Scientific Publishing; 2014.
[11] Merrett K, Fagerholm P, McLaughlin CR, Dravida S, Lagali N, Shinozaki N, et al. Tissue-engineered recombinant human collagen-based corneal substitutes for implantation: performance of type I versus type III collagen. Invest Ophthal Vis Sci 2008;49:3887–94.
[12] Fagerholm P, Lagali NS, Merrett K, Jackson WB, Munger R, Liu Y, et al. A biosynthetic alternative to human donor tissue for inducing corneal regeneration: 24-month follow-up of a phase 1 clinical study. Sci Transl Med 2010;2:46ra61.
[13] Dirk SM, Lin P, Buerger S, Cicotte KN, Reece GP, Hedberg-Dirk E. Biomimetic approaches to peripheral neuroprosthetic interfaces. In: Jabbari E, Kim DH, Lee LP, Ghaemmaghami A, Khademhosseini A, editors. Handbook of Biomimetics and Bioinspiration. Singapore: World Scientific Publishing; 2014. p. 121–51.
[14] Kim K, Hong S, Lee H. Mussel-inspired adhesive biomaterials. In: Jabbari E, Kim DH, Lee LP, Ghaemmaghami A, Khademhosseini A, editors. Handbook of Biomimetics and Bioinspiration. Singapore: World Scientific Publishing; 2014. p. 273–91.
[15] Liu W, Deng C, McLaughlin CR, Fagerholm P, Lagali NS, Heyne B, et al. Collagen–phosphorylcholine interpenetrating network hydrogels as corneal substitutes. Biomaterials 2009;30:1551–9.
[16] Hackett JM, Lagali N, Merrett K, Edelhauser H, Sun Y, Gan L, et al. Biosynthetic corneal implants for replacement of pathologic corneal tissue: performance in a controlled rabbit alkali burn model. Invest Ophthalmol Vis Sci 2011;52:651–7.
[17] Holzer MP, Rabsilber TM, Auffarth GU. Femtosecond laser-assisted corneal flap cuts: morphology, accuracy, and histopathology. Invest Ophthalmol Vis Sci 2006;47:2828–31.
[18] Saeidi N, Karmelek KP, Paten JA, Zareian R, DiMasi E, Ruberti JW. Molecular crowding of collagen: a pathway to produce highly-organized collagenous structures. Biomaterials 2012;33:7366–74.
[19] Lan S, Veiseh M, Zhang M. Surface modification of silicon and gold-patterned silicon surfaces for improved biocompatibility and cell patterning selectivity. Biosens Bioelectron 2005;20:1697–708.
[20] Qin D, Xia Y, Whitesides GM. Soft lithography for micro- and nanoscale patterning. Nat Protoc 2010;5:491–502.
[21] Fujikawa LS, Foster CS, Harrist TJ, Lanigan JM, Colvin RB. Fibronectin in healing rabbit corneal wounds. Lab Invest 1981;45:120–9.
[22] Nishida T, Nakagawa S, Nishibayashi C, Tanaka H, Manabe R. Fibronectin enhancement of corneal epithelial wound healing of rabbits in vivo. Arch Ophthalmol 1984;102:455–6.
[23] Yamada N, Morishige N, Yanai R, Morita Y, Kimura K, Chikama T, et al. Open clinical study of eye drops containing the fibronectin-derived peptide PHSRN for treatment of persistent corneal epithelial defects. Cornea 2012;31:1408–13.
[24] Priest D, Munger R. A new instrument for monitoring the optical properties of corneas. Invest Ophthalmol Vis Sci 1998;39:S352.
[25] Meek KM, Hayes S. Corneal cross-linking – a review. Ophthalmic Physiol Opt 2013;33:78–93.
[26] Zhou Y, Valiokas R, Liedberg B. Structural characterization of microcontact printed arrays of hexa(ethylene glycol)-terminated alkanethiols on gold. Langmuir 2004;20:6206–15.
[27] Araki-Sasaki K, Ohashi Y, Sasabe T, Hayashi K, Watanabe H, Tano Y, et al. An SV40-immortalized human corneal epithelial cell line and its characterization. Invest Ophthalmol Vis Sci 1995;36:614–21.
[28] Patel S, Marshall J, Fitzke 3rd FW. Refractive index of the human corneal epithelium and stroma. J Refract Surg 1995;11:100–5.
[29] Graham DJ, Price DD, Ratner BD. Solution assembled and microcontact printed monolayers of dodecanethiol on gold: a multivariate exploration of chemistry and contamination. Langmuir 2002;18:1518–27.
[30] Saeidi N, Sander EA, Zareian R, Ruberti JW. Production of highly aligned collagen lamellae by combining shear force and thin film confinement. Acta Biomater 2011;7:2437–47.
[31] Liu Y, Gan L, Carlsson DJ, Fagerholm P, Lagali N, Watsky MA, et al. A simple, cross-linked collagen tissue substitute for corneal implantation. Invest Ophthalmol Vis Sci 2006;47:1869–75.
[32] Bernard A, Delamarche E, Schmid H, Michel B, Bosshard HR, Biebuyck H. Printing patterns of proteins. Langmuir 1998;14:2225–9.
[33] Bernard A, Renault JP, Michel B, Bosshard HR, Delamarche E. Microcontact printing of proteins. Adv Mater 2000;12:1067–70.
[34] Fukuda J, Sakai Y, Nakazawa K. Novel hepatocyte culture system developed using microfabrication and collagen/polyethylene glycol microcontact printing. Biomaterials 2006;27:1061–70.
[35] PDMS (polydimethylsiloxane), 6.777J/2.751J Material Property Database, 2014. <http://www.mit.edu/~6.777/matprops/pdms.htm>.
[36] Murakami J, Nishida T, Otori T. Coordinated appearance of beta 1 integrins and fibronectin during corneal wound healing. J Lab Clin Med 1992;120:86–93.
[37] Shibue T, Weinberg RA. Integrin beta1-focal adhesion kinase signaling directs the proliferation of metastatic cancer cells disseminated in the lungs. Proc Natl Acad Sci USA 2009;106:10290–5.
[38] Diehl KA, Foley JD, Nealey PF, Murphy CJ. Nanoscale topography modulates cornea epithelial cell migration. J Biomed Mater Res A 2005;75A:603–11.
[39] Théry M. Micropatterning as a tool to decipher cell morphogenesis and functions. J Cell Sci 2010;123:4201–13.
[40] Maurice DM. In: Davson H, editor. The Eye. New York: Academic Press; 1962. p. 296.
[41] van den Berg TJ, Tan KE. Light transmittance of the human cornea from 320 to 700 nm for different ages. Vision Res 1994;34:1453–6.
[42] Beems EM, Van Best JA. Light transmission of the cornea in whole human eyes. Exp Eye Res 1990;50:393–5.
[43] Zeng Y, Yang J, Huang K, Lee Z, Lee X. A comparison of biomechanical properties between human and porcine cornea. J Biomechan 2001;34:533–7.
[44] Crabb RA, Chau EP, Evans MC, Barocas VH, Hubel A. Biomechanical and microstructural characteristics of a collagen film-based corneal stroma equivalent. Tissue Eng 2006;12:1565–75.
[45] Jue B, Maurice DM. The mechanical properties of the rabbit and human cornea. J Biomechan 1986;19:847–53.